J Comp Physiol (1981) 145:209–226

Journal
of Comparative
Physiology · A

Optics of the Eyes of *Phronima* and Other Deep-Sea Amphipods

M.F. Land
School of Biological Sciences, University of Sussex, Brighton BN1 9QG, England

Accepted September 15, 1981

Summary. 1. *Phronima*, and many other oceanic hyperiid amphipods, have double eyes in which the medial (dorsal) part has a small field of view and large facets, and the lateral (ventral) part a large field and small facets (Fig. 6).

2. The eyes are of the apposition type. Each crystalline cone forms an image at its proximal tip (Fig. 3), which in most hyperiids abuts directly onto the rhabdom. The exception is the medial eye of *Phronima* where light from the image is conveyed via a narrow light-guide to the retina 5 mm ventral to the eye surface (Fig. 2). Living eyes all show pseudopupils (Fig. 4).

3. It is shown by interference microscopy that the crystalline cones in *Phronima* eyes are inhomogeneous (Figs. 7–8, 11–13). Medial eye cones have a V-shaped refractive index gradient, densest at the distal tip (1.40). Lateral cones are dense at both distal (1.38) and proximal (1.45) ends, with a less dense zone in between. Ray tracing (Figs. 9 and 13) confirms that images are formed at the proximal ends of both types of cone.

4. Measurements made on the pseudopupil and from ray tracing confirm that in the medial eyes the acceptance angles of single light-guides are larger than the inter-ommatidial angles by a factor of 8 ($\Delta\rho = 3.5°$, $\Delta\phi = 0.44°$). This means that as many as 60 rhabdoms in each medial eye view the same point in space. There is no such discrepancy in the lateral eyes, where $\Delta\rho \simeq 15°$ and $\Delta\phi$ is 9–12°. The entire field of view of each medial eye (approximately 10.5 by 11°) is about the same as that of a single ommatidium in the lateral eye.

5. It is argued in the Discussion that, whilst a high $\Delta\rho : \Delta\phi$ ratio would be a disadvantage if a textured background had to be resolved, it is a good solution to the problem of locating single small objects in dim light, *provided* that all the rhabdoms that view the same point in space pool their signals. A substrate for such pooling appears to exist in a plexus overlying the lamina of the medial eye, which is not present in the lateral eye lamina (Fig. 16).

6. The structure of the eyes of the deep-living *Cystisoma*, which has no lateral eyes, differs from *Phronima* in that the retina is curtain-like, with widely separated, unscreened rhabdoms, instead of being a small dark condensed structure. It is suggested that these represent alternative ways of making eyes that are minimally visible to potential predators (Fig. 17).

Introduction

Because of the difficulties of seeing in the dim light of the deep sea, many of the animals that inhabit this environment have evolved large eyes with a high light-gathering power. The fish and cephalopods have hypertrophied eyes, which are often tubular, the field of view restricted to a relatively small upward-directed region (Lythgoe 1979; Marshall 1954; Lockett 1977). The eucaridan crustaceans, like some nocturnal insects, have superposition compound eyes with wide effective apertures. These are based on a mirror arrangement in the decapod shrimps, and on lens-cylinders in the euphausiids and the peracaridan mysids (Land 1980a). Another family of Crustacea, the hyperiid amphipods, have exploited the possibilities of the more familiar apposition compound eye in which each rhabdom has its own private lens system, and their eyes are the subject of this paper.

Most mid-water hyperiids have large and remarkable eyes. *Phronima sedentaria*, one of the commoner and best studied members of the group, is a moderately large (20–30 mm), very transparent animal whose head is almost all eye. It has in fact four eyes, two small ones with wide fields of view located ventrally, and another much larger pair whose optics occupy

0340-7594/81/0145/0209/$03.60

the whole of the top of the head. These upper eyes are especially odd in that each of the 800 or so lenses channels light into a narrow (10–20 μm) light-guide leading to a rhabdom in the ventrally situated retina, 5 mm away (Claus 1879; Exner 1891; Ball 1977). Although *Phronima* is extreme in the way its eyes are partitioned, most of the hyperiids show some degree of dorso-ventral specialization in eye structure.

As far as the optical properties of these eyes are concerned the only relevant study is Exner's (1891; pp. 130–135). In this he showed that light entering the lenses of the dorsal eyes was focused into the light-guides, and that light passed down these guides even in celloidin embedded material. He also worked out that the curvature of the distal surface of each lens was not enough in itself to bring light to a focus at the light-guide tip, and that therefore the lenses (crystalline cones) must have an internal refractive index gradient to supplement the focusing power of the surface. In this he was quite correct (Fig. 8b), though at the time this was speculation. One of the aims of this paper is to measure the refractive index gradients in the lenses and to reconstruct their focusing properties.

The second aim is to provide basic information about those parameters of eye design that are important in trying to assess what the eye can see, for example the inter-ommatidial angles ($\Delta\phi$), the acceptance angles of single ommatidia ($\Delta\rho$) and the fields of view of the different eyes. The present study was facilitated by the discovery that in life these eyes do have an easily visible pseudopupil – the black spot which, as in an insect eye, indicates the location of those ommatidia that share a common line of sight with the observer (Fig. 4). Pseudopupil measurements permit the lines of sight of different ommatidia to be mapped onto the angular space around the eye (cf. Horridge 1978) and hence the inter-ommatidial angles and fields of view can be measured. Acceptance angles can be obtained both from a knowledge of the way the lenses focus light, as well as from the pseudopupil size.

Equipped with this information I have tried in the Discussion to relate some of the peculiarities of these eyes (large facets, large acceptance angles but very small interommatidial angles in the medial eyes) to the task that they probably fulfil, namely the detection of small objects against a dim background.

Materials and Methods

Living amphipods were collected from midwater trawls in the N. Atlantic at depths from the surface to 1,000 m, during cruises 77 (1976) and 105 (1979) of the R.R.S. Discovery. Those that were not examined immediately were fixed, usually in a mixture of 3% glutaraldehyde and 4% formaldehyde in sea-water. It was found that with this fixative the optical structures retained their transparency and did not measurably change their dimensions. The average refractive indices of fresh crystalline cones, estimated from their focal length for light passing through them sideways, was in the same range (1.36–1.38) as that measured months later by interference microscopy on fixed cones. It is therefore assumed that fixation on its own has a negligible effect on the optical properties of these structures.

Methods used to study pseudopupils and image formation are described in the Results section.

Interference microscopy was performed using the Baker shearing interference version of a Vickers M41 microscope. The instrument produces two beams of light, one of which passes through the specimen and the other through the surrounding medium (sea water). The beams are recombined in the objective and give rise to interference patterns that represent path difference contours in the specimen. Thus, if the background is dark the 1st light band will occur when the path difference is $\lambda/2$, the first dark band when it is λ and so on ($\lambda = 542$ nm). For the m'th dark band the path difference is $m\lambda$, so that:

$$\text{p.d.} = m\lambda = t(\bar{n}_s - n_m), \quad \text{or} \quad \bar{n}_s = \frac{m\lambda}{t} + n_m,$$

where t is the local thickness of the specimen, n_m is the refractive index of the medium (1.34) and $\bar{n}_s$ is the *average* refractive index of the specimen. The local thickness can be obtained by measurement, assuming the cross section of the crystalline cones to be circular, so that $\bar{n}_s$ is readily obtained.

Interference micrographs of whole mounts are not easy to interpret, and the preferred method is to take thin sections where each zone can be thought of as having a constant refractive index and producing no bending of light rays (Hausen 1973). The softness of the tissue in *Phronima* precluded reliable section cutting (Fig. 7c), so that refractive index profiles had to be reconstructed from the whole mount photographs (Figs. 7a, b and 11a–c). The first problem is that, if the structures are inhomogeneous, $\bar{n}_s$ is not the actual refractive index anywhere, but the average of the contributions of all the different zones in the structure. To overcome this each cross section was divided into 5 or 10 zones, as shown in Fig. 1a, and $\bar{n}_s$ was determined at distances from the axis corresponding to the centre of each zone. The outermost zone was assumed to be homogeneous, so that $n_1 = \bar{n}_1$, and n_2 was then calculated from $\bar{n}_2$ by subtracting out the component contributed by the n_1 layer. n_3 etc. were calculated similarly. Thus from Fig. 1a:

$$0.72\,\bar{n}_2 = 0.39\,n_2 + 0.33\,n_1$$

so that

$$n_2 = (0.72\,n_2 - 0.33\,n_1)/0.39$$

and

$$n_3 = (0.87\,\bar{n}_3 - 0.24\,n_1 - 0.295\,n_2)/0.335 \ldots \text{ etc.}$$

This procedure permits the reconstruction of the refractive index profile through the specimen at each level, and it successfully reproduced the index distribution in a homogeneous glass rod and a SELFOC light guide with a roughly parabolic refractive index gradient (Fig. 1b).

There is, however, a further problem with inhomogeneous structures with large index gradients, which is that the path of rays through the material is not straight (as implied in Fig. 1a) but slightly curved, and ideally the ray curvature should be allowed for. To make systematic corrections for this effect without first knowing the gradient of refractive index is extremely difficult, and so instead a 'worst case' gradient was constructed to see whether

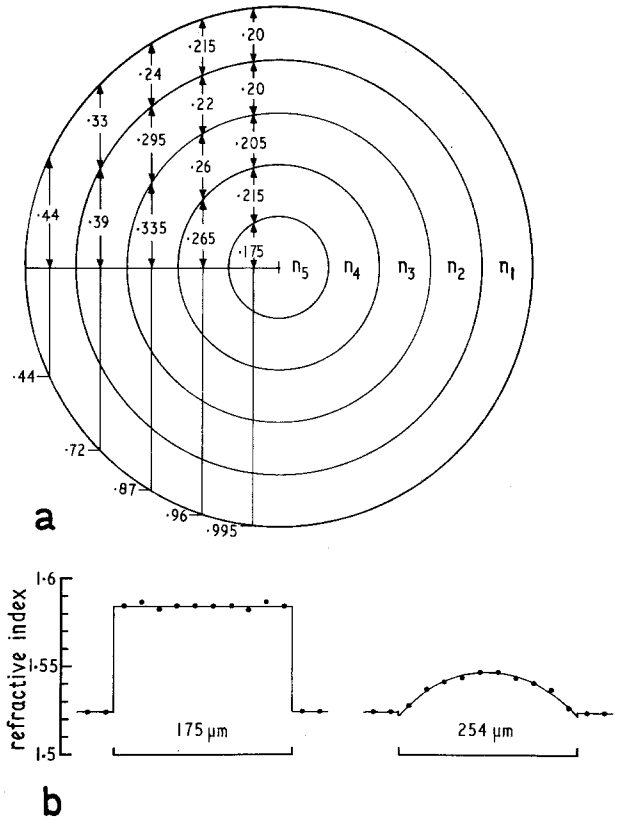

Fig. 1. a Proportions of a circular cross section used to calculate refractive index profiles from average refractive indices measured through the whole structure (see text). **b** Refractive index profiles for a homogeneous glass rod (*left*) and graded index (SELFOC) fibre, using the method described in the text and Fig. 1a. Both are derived from interference micrographs taken in immersion oil ($n=1.524$). The manufacturers' estimate of the refractive index range in the SELFOC fibre (0.025) is the same as that obtained here (Koizuma et al. 1974)

the errors resulting from the method given above could be safely ignored. Ray paths were worked out through a structure with a parabolic refractive index gradient ranging from 1.41 on axis to 1.33 peripherally. The total path lengths were summed, and these were used to reconstruct the fringe pattern that would have been seen with the interference microscope. This was then analysed using the method given, to reconstruct the gradient. There was a small amount of distortion. In particular the calculated refractive index in the outer middle zones (n_2 and n_3) was about 0.005 higher than it should have been, and the central index (n_5) was similarly depressed. This means that the refractive index profiles and contour maps given here (Figs. 8 and 13) are accurate to the 2nd decimal place, but probably not the 3rd. The effects of these errors on ray tracings (Figs. 9 and 14) are negligible.

A useful taxonomic guide to hyperiid genera is provided by Bowman and Gruner (1973).

Results

Anatomy of Phronima Eyes

Medial Eyes. In a moderately large specimen of *P. sedentaria* (25 mm) there were 390 facets in each medial eye (Fig. 4). The cornea is flat, and the hexagonally facetted appearance is due to the crystalline cones beneath it. These are circular in surface view, with a diameter of 135 μm over most of the eye surface, though falling to about half this at the extreme edges of the eye. In one large specimen cone diameters reached a maximum of 185 μm. In living animals the crystalline cones are almost contiguous, with a gap of not more than 10 μm between them: this is interesting because in alcoholic fixatives (but not aqueous ones) they shrink to about half their initial diameter leaving a wide gap between them (cf. Ball 1977, Fig. 3). Presumably alcoholic dehydration would have an equally severe effect on their optical properties. When freed from the cornea the cones are seen to have a characteristic shape (Figs. 2c and 7a); the distal tip is elliptical in profile, the body of the cone tapers gradually (~10°) for 0.3 to 0.5 mm, then more steeply (~15°) for about the same distance before merging into the light-guide portion. In the specimen with 135 μm diameter cones the light-guides have diameters of 13.0±2.2 (s.d.) μm, and 17.6±3.6 μm in an animal with 185 μm cones. Thus the ratio of area of the crystalline cone aperture to that of the light guide (and hence the rhabdom, which has the same diameter) is about 110:1 in both cases. In life the light-guides are aligned with the axes of the corresponding cones and run quite straight to the retina situated 5 mm ventral to the eye surface (Fig. 2b). There each light guide abuts directly onto the tip of its rhabdom (Ball 1977, Fig. 11). The rhabdoms may be as much as 350 μm long (Ball 1977). There is no screening pigment at all in the region of the crystalline cones and light-guides until the latter reach the retina. Pigment then shields their proximal tips, and the rhabdoms from each other.

Lateral Eyes. In contrast to the medial eyes which cover a narrow angle and have their optics well separated from the retina, the lateral eyes each have a field of view of roughly 180° in both longitudinal and transverse planes, and the crystalline cones encircle the retina. There are no light-guides. The cones, which are rather different in shape from those of the medial eyes (Fig. 11) contact the rhabdoms directly. There are about 19 rows of cones covering 180° in the transverse (dorso-ventral) plane and about 15 rows covering a similar angle in the longitudinal plane, the total number of ommatidia being about 250 per eye. Based on the alignment of the cone axes, the inter-ommatidial angles are in the range 9–12°. By the same anatomical criterion the inter-ommatidial angles for the medial eyes are less than 1° (see below). The lateral eye cones vary in length with position in the eye from 400 μm (upwards and downwards)

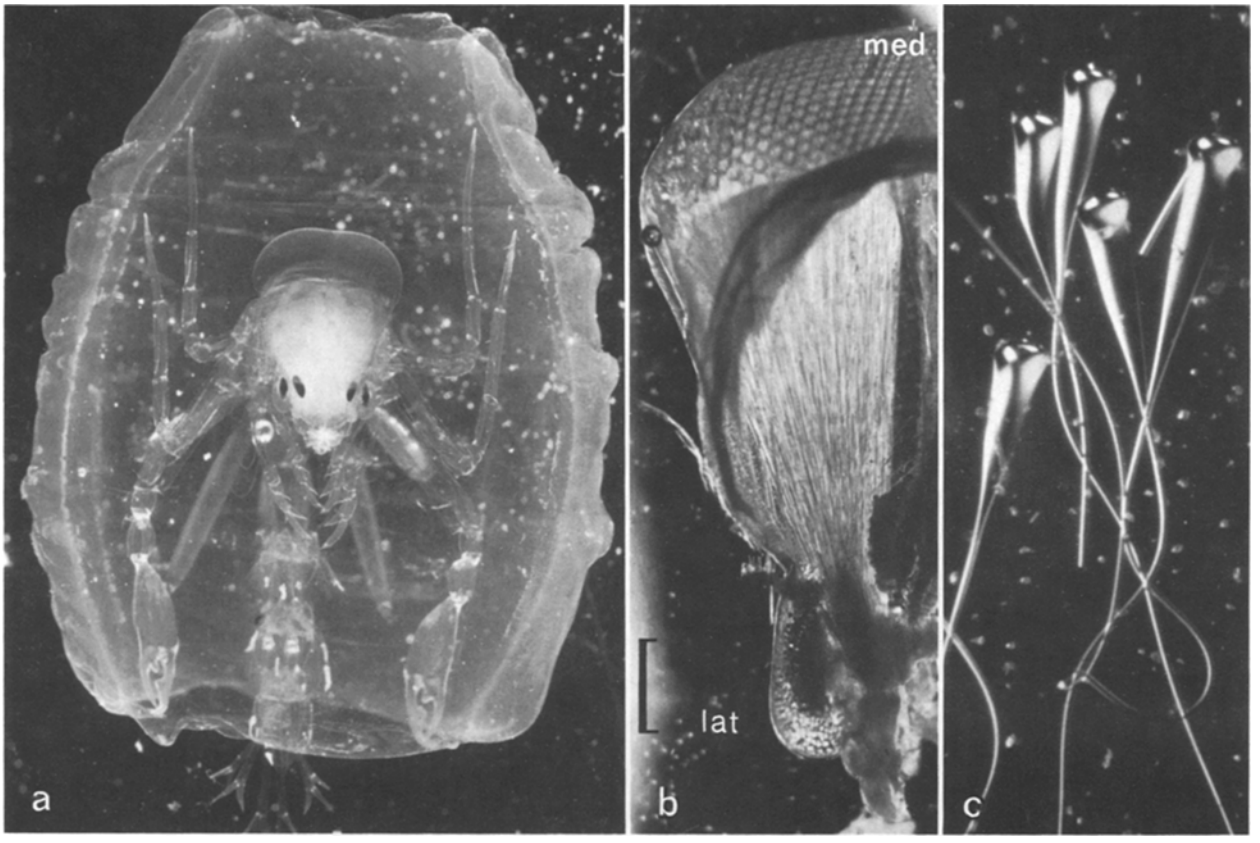

Fig. 2. a *Phronima sedentaria*. Whole living female in a characteristic posture in its barrel, which it makes from the test of a tunicate. The barrel is 25 mm long and the animal's head is 7.4 mm from top to bottom. The four black dots are the retinae; the outer 2 belonging to the small tear-like lateral eyes, and the inner 2 to the medial eyes, whose optics cover the whole dorsal surface of the head. **b** Head of *Phronima* separated from the body and viewed from behind, showing the light-guides which join the crystalline cones to the retina. *Med* medial eye; *lat* lateral eye. *Scale bar*: 1 mm. **c** Isolated fixed crystalline cones from the medial eye, showing their shape, and the continuity of cone and light-guide. The largest cone is 185 μm in diameter at its distal tip, and just less than 1 mm long. Dark field illumination

to 200 μm laterally. They are widest at their distal tips (about 100 μm) then cylindrical (60–80 μm diameter) for half their length before tapering down to about 25 μm at the point where they enter the retina. According to Ball (1977) the rhabdoms are shorter in the lateral eyes than in the medial, in the range 50–200 μm, and up to 30 μm wide. As in the medial eyes, there is no screening pigment distal to the retina.

Other details of the anatomy and cytology of the eyes, and references to the earlier literature, are given in Ball's 1977 paper.

Image Formation by Crystalline Cones in the Medial Eyes

If the dorsal eye functions as an ordinary apposition eye one might expect that the crystalline cones each focus an image of a small region of outside space onto the distal ends of the light-guides. The problem of trying to see whether images are formed is basically that the cones, even when fixed, are very soft and flexible, and must be studied in situ so that they retain their alignment. This was achieved by cutting off the whole head, positioning it so that the eye viewed a target (Fig. 3), and examining the image in the most posterior cones adjacent to the boundary with the thorax. For more central cones the images are invisible because the forest of light guides obstructs the view.

Figure 3 shows images of an object (an A) formed by these cones. The object lay about 10° to the side of the cone axes so that the images do not pass down the light-guides, but are formed in the water adjacent to region where the cones and light-guides merge. The images are inverted, meaning that each crystalline cone is behaving as a single simple lens. Some are distorted, but those formed nearest to the light-guides are clearly of good quality. An estimate of the focal length (posterior nodal distance) of a cone can be made from the image magnification. The object was

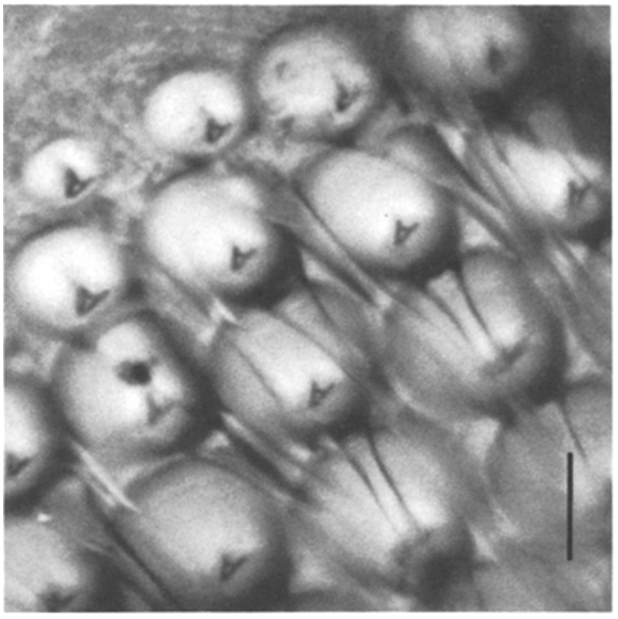

Fig. 3. Photograph of inverted images of the latter A produced by cones near the posterior edge of the eye. The images are focused in the water adjacent to the light-guides, and at the level of the point of merger of cone and light-guide. *Scale bar*: 100 μm

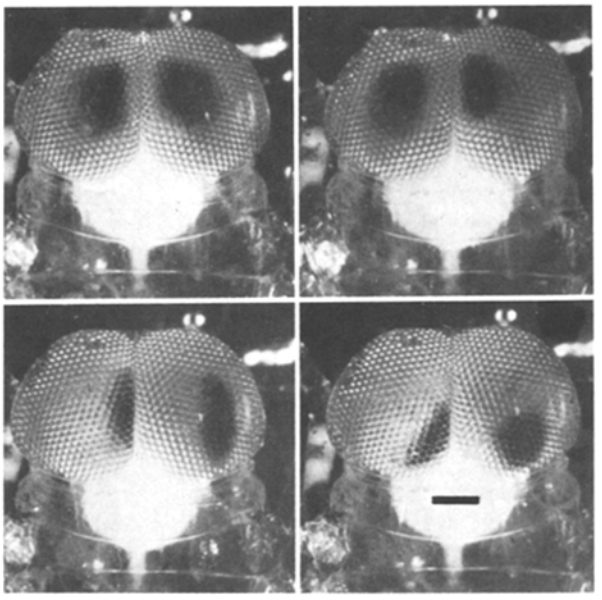

Fig. 4. Four views of the pseudopupil in the medial eye, taken through a narrow aperture (1°). The central pseudopupil (*top left*) covers about 60 ommatidia, and has an angular width of about 4°. Note the changes in size and shape of the pseudopupils as the animal is tilted slightly, and the large extent of the binocular field over which 2 pseudopupils are visible. *Scale bar*: 1 mm. Living animal

6 mm high, and situated at a distance of 47.5 mm, in water, in front of the cornea. The best images in Fig. 3 are 24.8 μm high. The focal length for these cones (diameter 151 μm) is thus $\frac{47.5 \times 0.0248}{6}$ mm, or 196 μm. Taking this figure, and assuming that only light focussed within the distal tip of each light-guide travels to the retina (an assumption that is not entirely valid since some light will be reflected in from the walls of the cone) then a 15 μm light-guide would image light from 15/196 radians of visual space, or 4.4°.

This result is in good agreement with values of about 4° for the acceptance angle $\Delta\rho$ from pseudopupil and ray-tracing studies, but this is slightly fortuitous. The cones in this part of the eye are shorter than in the centre, and presumably have shorter focal lengths, and this approximately cancels the effect of the assumption that only imaged light enters the light guide (see Fig. 10). Nevertheless these observations show that the crystalline cones are image-forming devices, and that their images are formed at the level of the junctions between cone and light-guide.

A Demonstration of Apposition Optics

If the medial eye of a living animal is illuminated with a small light source several cm from the eye, a small patch of the retinal surface, viewed from the side, can be seen to glow bright red from light scattered and reflected by the retinal screening pigment. As the light source moves this patch of light also moves, and the whole retina is traversed by an anteroposterior rotation of the light around the animal of 13.5°. This shows that light from different regions of external space stimulates different regions of the retina. When a pin is moved across the surface of the eye, so as to occlude a few rows of ommatidia aligned with the light source, the retinal glow is obliterated. This would not happen if the eye was of the superposition type, where one would expect the whole eye surface to contribute to the image at each retinal point. It confirms the view that each ommatidium acts as a unit that images a small solid angle of outside space.

The Pseudopupil in the Medial Eyes

Appearance. When the medial eye is observed from above (dorsally) along a direction that coincides closely with that of the cone axes and light-guides, a large conspicuous black spot appears in each eye (Fig. 4). These spots move across the eye surface when the animal is tilted slightly, they do not correspond to any physical object in the eye (they are much larger than the retina, for example) and their size and sharpness are relatively insensitive to the plane of focus.

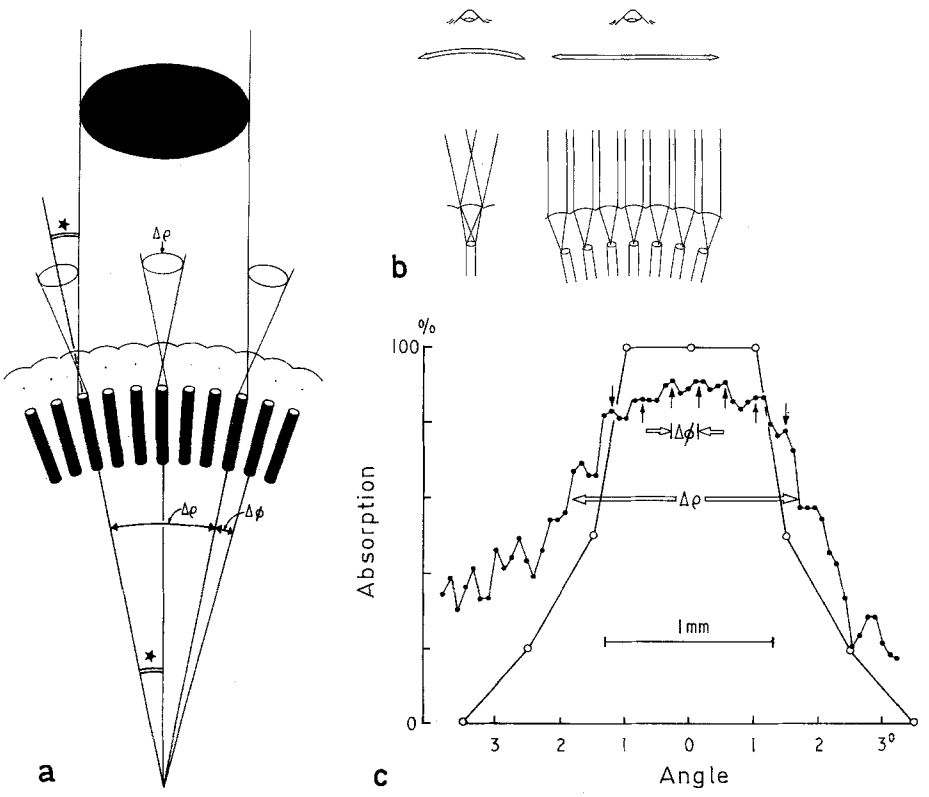

Fig. 5. a Geometry of the pseudopupil. The pseudopupil will be seen over an area of the eye surface that corresponds to an angle of $\Delta\rho$ at the local centre of curvature of the eye, where $\Delta\rho$ is the acceptance angle of a single rhabdom, or in this case light-guide. The proof is that the two indicated angles (*) are equal. This is only strictly true if there is no screening pigment in the image plane of the crystalline cones, as is the case in *Phronima*. **b** Alternative methods of studying the acceptance function of the light-guides. *Left*: By rotating microscope around one facet, or rotating the animal. *Right:* By scanning across an array of facets. **c** Acceptance function of a light-guide measured by scanning across a Kodachrome photograph of the pseudopupil (Fig. 4) using a densitometer (*solid dots*). The width of $\Delta\rho$, measured at half the maximal absorption, is 3.5°. The interommatidial angle, from the small fluctuations due to the facets, is 0.44°. The curve with open circles is the acceptance function of a light-guide estimated by ray tracing (Fig. 10): this has a width of 3°

The only possible explanation is that they are pseudopupils, and that as in insect eyes they represent that region of the eye surface that is absorbing light from the direction of observation (rev. Stavenga 1979). If a facet appears black, this means that it is behaving as a light sink for light from the direction of observation, and since there is no absorbing pigment distal to the retina this in turn means that all the light entering such a facet finds its way to the retina, via the connecting light-guide. Notice that in the centre of the pseudopupil each facet is dark across its entire diameter, which means that all on-axis light reaching the distal surface of the crystalline cone must enter the light-guide, i.e. that the crystalline cone is an effective collector or condenser lens for the light-guide, as might be expected from its image-forming properties. Even when the camera is fully stopped down so that it accepts light from less than a 1° angle, the pseudopupil remains large, and cannot be reduced to a diameter smaller than about 1/3 of the diameter of the eye, or about 8 facets along a row. The number of facets enclosed by a centrally positioned pseudopupil is about 60, and this must also be the number whose acceptance angles ($\Delta\rho$) include the direction of observation (Figs. 5a and 15b). 60 facets look at the same point in space.

A pseudopupil is also visible in the lateral eyes, but this is very small, only 1–2 facets wide. This is a larger *angular* extent (~20°) than in the medial eyes (~4°; see below) but there is nothing like the same degree of overlap between facets.

Fields of View. As one rotates a *Phronima* in a dish of sea water while examining the medial eye the pseudopupil moves across the eye and finally disappears off the edge. This disappearing point must mark the edge of the field of view, since the retina is no longer absorbing light. The extent of the fields of view, measured in this way with the end point taken as the position where the centre of the pseudopupil is aligned

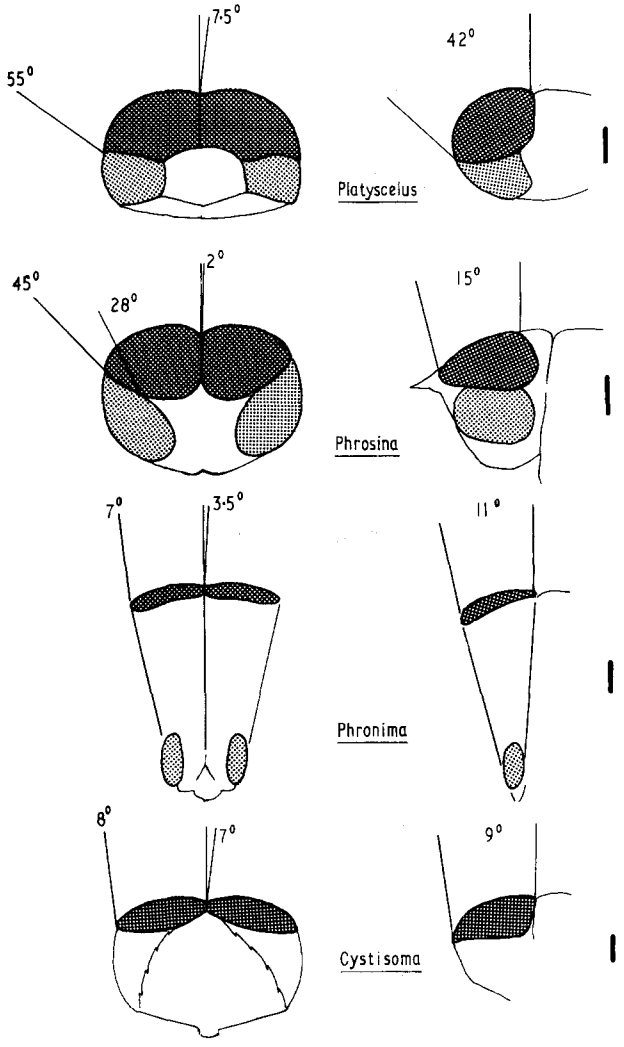

Fig. 6. Fields of view of the medial eyes of 4 deep-sea hyperiids (*Platyscelus ovoides, Phrosina semilunata, Phronima sedentaria* and *Cystisoma* sp.) determined from the positions at which the pseudopupil is half visible. Ipsi- and contralateral fields are shown on the frontal view, and all have some overlap. In *Platyscelus* and *Phrosina* the fields of the medial and lateral eyes are contiguous, as shown by pseudopupil continuity. The medial eyes (*heavy stipple*) have larger facets than the lateral eyes (*light stipple*) and have separate retinae. *Cystisoma* has no lateral eyes (Fig. 17). *Bars:* 1 mm

with the marginal facet, are shown in Fig. 6 for *Phronima* and 3 other hyperiids. The ipsilateral field of each medial eye in *Phronima* extends to 7° and the contralateral to 3.5° in the transverse (dorso-lateral) plane, so that there is a 7° region of binocular overlap. In the sagittal plane the field is 11° from front to back. If total disappearance of the pseudopupil is taken as the criterion, the corresponding figures are 11.5°, 4°, 8° and 14.5°. The former measure defines the field in terms of the optical axes of the ommatidia, and the latter should give the extreme limits over which the medial retina receives light. The remarkable feature of these results is the narrowness of the fields of view, probably the smallest of any compound eye, except *Cystisoma* (see Discussion).

Acceptance Angle ($\Delta\rho$) and Interommatidial Angle ($\Delta\phi$). Because there is no pigment outside the retina one can be reasonably confident that the width in angular space of the pseudopupil is the same as the width of the acceptance function of a single light-guide, and hence of the single rhabdom at its base. Once in the light-guide, rays will be multiply reflected until absorbed at the base, but the pigment configuration at the base will not affect the acceptance function of the distal end of the guide, where the image lies, nor the appearance of the pseudopupil. This is different from the situation in other Crustacea and insects with apposition eyes where both rhabdom photopigment and surrounding screening pigment lie in the focal plane of the lens, and where both contribute to the form of the pseudopupil (Stavenga 1979).

If one examines a single facet in the centre of a median eye, and rotates the animal so that the pseudopupil completely traverses that facet, the angle turned is approximately 4°. Alternatively, the distance moved by the pseudopupil across the eye can be measured for a given angular rotation of the animal, and this figure can be used to estimate the angular width of the pseudopupil directly from photographs. The result is given in Fig. 5c where a photograph was scanned with a densitometer, and it shows that the width of the pseudopupil between the points of half-maximal absorption is 3.5°. This should mean that the acceptance angle of the light-guides is also 3.5°.

On the same plot, in Fig. 5c, it is also possible to see small bumps that correspond to the individual facets along a single row. Their angular separation is the interommatidial angle ($\Delta\phi$) and this is 0.44°. This figure, which was almost the same for 3 animals studied, is again remarkable in being smaller than in all other arthropods except some dragonflies where $\Delta\phi$ is as little as 0.24° (Sherk 1978). The other unusual feature is the enormous overlap between adjacent ommatidia. The ratio of $\Delta\rho:\Delta\phi$ is 8:1, whereas typical values for diurnal insects are around 1:1 (e.g. in the mantis; Rossel 1979). This degree of overlap between ommatidial fields of view, apparently representing redundant or unusable resolution, clearly needs some explanation (see Discussion).

Towards the edges of the eye the pseudopupil changes in size and shape (Fig. 4), and moves more slowly as the animal is rotated. These changes are consistent with interommatidial angles that are larger than in the centre of the eye, probably by a factor of about 2, but these variations have not been studied systematically.

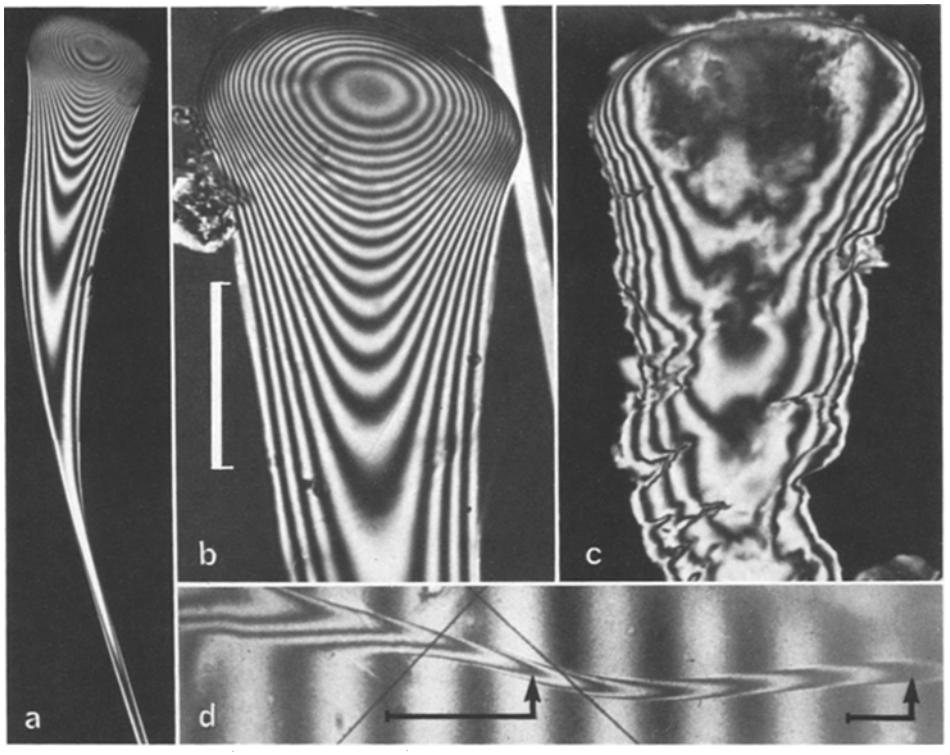

Fig. 7. a Interference micrograph, taken in sea water, of a whole fixed cone and beginning of the light-guide from the medial eye of *Phronima*. **b** Enlarged view of the distal region of a cone. *Scale bar*: 100 μm. **c** 50 μm thick frozen section of a cone on the same scale as **b**. Note the similarity to the refractive index contours in Fig. 8b. **d** Fringe-field interference micrograph of the region where the cone merges into the light-guide, showing the larger fringe displacement (1.7 wavelengths) and hence higher refractive index in the junction zone than further down the guide (0.8 wavelengths)

The Internal Structure and Focusing Properties of the Crystalline Cones

To study the focusing properties of the cones in detail it is necessary to measure their internal refractive index structure, and then to calculate ray paths through the refractive index profiles. It is clear that the cones must be inhomogeneous. The distal tip of a large cone has a radius of curvature of about 130 μm, and the refractive index in this region is around 1.4 (see below). The focal length for a homogeneous structure would then be given by the usual formula for single surface refraction: $f=n_1 r/(n_2-n_1)$, where n_1 is 1.34 (sea water). This gives a focal length of 2.9 mm, which is greater than that obtained by direct measurement of the image (Fig. 3) by more than an order of magnitude. The conclusion must be that focusing is achieved by continuous bending within the cone, as in *Limulus* (Land 1979) and many other arthropods (Exner 1891; Kunze 1979).

The procedure adopted was to take interference micrographs of single cones which were fixed but otherwise untreated (Fig. 7). From these, refractive index profiles were obtained as described in the Methods section. These results are plotted as profiles in Fig. 8a, and as contour lines of refractive index drawn on a central section of the cone in Fig. 8b. The latter can be used for ray tracing directly, either by applying Snell's law at each contour interval, or by calculating the radius of curvature of the ray (Meggitt and Meyer-Rochow 1975) when the ray runs parallel to a contour. The results are shown in Fig. 9.

On their own the interference micrographs are not easy to interpret because of the confusion of refractive index and thickness. They do show, however, that at the tip of a large cone (183 μm diameter) there are 19 fringes, so that the average refractive index is 1.396. Halfway down the cone there are 4 fringes and the diameter is 120 μm, so that the average index is 1.358. The cone is optically most dense at its distal tip. The refractive index of the light-guides cannot be measured accurately by the 'flat-fringe' technique because the path differences are less than a wavelength. However, if the microscope is arranged to have narrow fringes in the field of view, the extent of their distortion can give the average refractive index of the threads. This lies between 1.354 and 1.359 over most of their length. This technique also shows that in a short region around the junction of cone and light guide the refractive index is much higher,

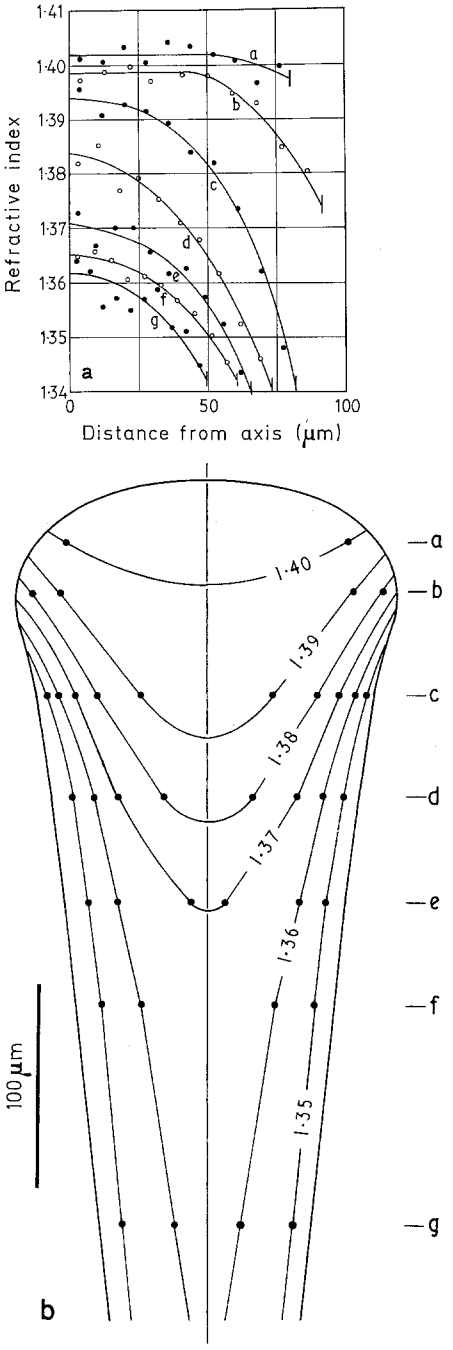

Fig. 8. a Calculated refractive index profiles through a cone like that shown in Fig. 7b at the levels shown in Fig. 8b. A 10-zone construction (cf. Fig. 1a) was used in the calculation. The distal region has a high and almost uniform refractive index, which progressively becomes lower and more parabolic proximally. **b** Refractive index contours in a central section of a cone, plotted from the data in **a**. Compare with the section shown in Fig. 7c

about 1.39 (Fig. 7d). Because of its short length (200 μm) this high index portion is not likely to affect the focusing properties of the cone, but it may increase the critical angle for total internal reflection locally, so that more light is reflected into the thread.

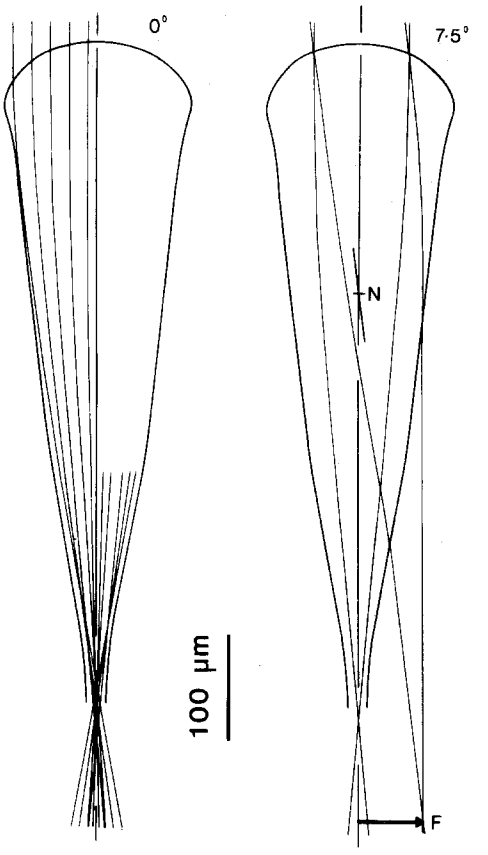

Fig. 9. *Left*: Tracing of the paths of paraxial rays through a central section of a cone, showing the focusing of rays into the light-guide. Constructed by applying Snell's law at the contours in Fig. 8b, and assuming that in the proximal third the refractive index rises uniformly to 1.39. *Right*: Sample off-axis rays showing that they focus outside the light-guide (see Fig. 3). *N* approximate position of the nodal point of the cone

The calculated refractive index profiles and contours for the distal 2/3 of a cone are shown in Fig. 8. The most striking features are first the longitudinal gradient along the axis, with the index falling from 1.4 at the distal tip to about 1.36 proximally, and second the presence of a transverse gradient. This transverse gradient is not present at the tip, where the refractive index is almost uniform (level a), but by level c this has become an almost parabolic gradient falling from 1.393 on the axis to about 1.342 peripherally, only slightly denser than the surrounding water. This pattern is similar at more proximal levels (d–g) except that the central index is lower, and the whole profile correspondingly flattened. The contours that result from the profiles in Fig. 8a are a series of increasingly steep V's (Fig. 8b). Although these are inhomogeneous structures, the lenses differ from classical lens-cylinders (Exner 1891; Kunze 1979) in not having cylindrical symmetry. Rays entering the cone thus encounter the descending series of

contours at an angle, rather than starting parallel to them. The other notable feature of these cones is their low refractive index, even in the densest part; the cones in *Limulus*, for example, have a central index of 1.51 falling to 1.44 (Land 1979) and the maximal indices in the cones of the superposition eyes of fireflies, moths and euphausiids are similar to that in *Limulus* (Land 1980a). This is no doubt related to the softness of *Phronima* cones, since refractive index is closely related to the concentration of material in a solution.

The correctness of the overall contour pattern in Fig. 8b can be checked by examining longitudinal frozen sections of the cones (Fig. 7c). Such sections show the refractive index profile directly in the pattern of fringes, because they have a uniform thickness and are thin enough for the gradient within them to be negligible. They are difficult to cut because the tissue remains soft even when fixed, and they tend to break up. The 50 μm section in Fig. 7c does, however, show the expected pattern, with an almost uniform distal region, drawn out into a series of V's proximally. This qualitative confirmation is valuable, but cutting sections is not a generally useable method with this material.

In the proximal 1/3rd of the cone the refractive index begins to rise again, and reaches a sharp peak (1.39) at the point where the cone becomes the light-guide. Because the cone is so narrow here it is not possible to obtain reliable information about the profile, if there is one, within it. The assumption made in the ray tracing that follows is that the refractive index in this region is uniform across the cone. In fact most of the focusing has been done by the distal part of the cone, and whatever assumptions one makes about this region they only cause the position of the focus to shift along the axis by a few tens of μm.

The ray tracings (Fig. 9) show that the effect of the gradient in Fig. 8 is to bring light reaching the distal tip of the cone to an approximate focus at the tip of the light-guide. Light rays furthest from the axis tend to meet the refractive index contours at the shallowest angles, and so are bent relatively more than rays close to the axis. The result is that all paraxial rays intersect within a longitudinal spread of about 100 μm, and almost all the light that enters the cone reaches the light-guide – as would be expected from the appearance of the pseudopupil. Rays that are more than a few degrees off axis do not enter the light-guide, but leave the cone at some point and are brought to a focus outside the structure (Fig. 9). It is rays such as these that form the images visible in Fig. 3. The nodal point (N) of a cone can

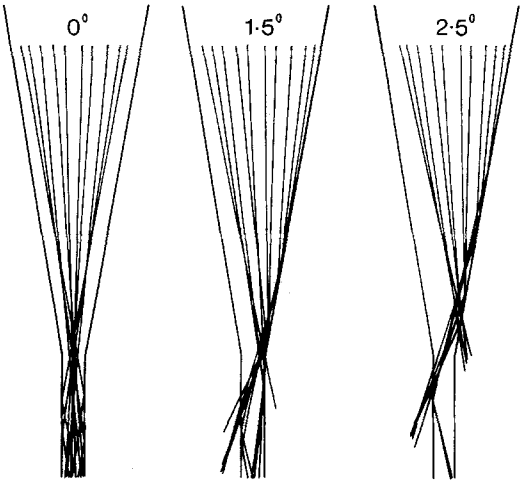

Fig. 10. Construction showing that rays may enter the light-guide after 0, 1 or 2 internal reflections at the cone/light-guide wall, depending on the initial angle of the parallel bundle at the cone's distal surface. The number of rays surviving reflection is used to construct the acceptance function in Fig. 5c. The refractive index is assumed to be 1.39 in this region

be found approximately by drawing a line through the image tip, parallel to the original direction of the image-forming rays. The focal length for axial rays is then the distance from the nodal point to the on-axis image, which in the cone illustrated is 403 μm. This is twice the focal length obtained from image magnification in the marginal cones, but when their smaller size is taken into account the agreement is quite good.

Based on a focal length of 403 μm, and an average diameter for the light-guides of 17.6 μm, one would expect each light-guide to image an angle in outside space of 17.6/403 radians, or 2.5°. This, however, is likely to be an underestimate of the acceptance angle ($\Delta\rho$) because some light is reflected into the light-guide from the walls of the cone. An attempt to estimate the size of this effect is given in Fig. 10. In the figure the bundle of image-forming rays has been rotated around the nodal point, and then each ray 'tested' when it reaches the cone/medium interface to see whether or not it will be reflected back into the cone or light-guide. The criterion is that the ray should make an angle with a normal to the interface that is greater than the critical angle at the point of incidence. The critical angle is given by $\sin^{-1}(n_{out}/n_{in})$ where n_{out} is the index of sea water (1.34) and n_{in} that of the cone in this region. Thus at the junction of cone and light-guide n_{in} is 1.39 and the critical angle 75°, so that rays making angles smaller than 15° with the wall will be totally internally reflected, and those making larger angles will pass

through. The figure shows that on axis all rays enter the light-guide, by 1.5° off axis 9 of the 10 rays are reflected once, but only 5 survive the second reflection, and by 2.5° off axis only 2 remain in the guide after the second reflection. This permits one to draw a very approximate acceptance function for the light guide if it is assumed that all rays that survive the second reflection remain in the guide. This is plotted in Fig. 5c where it is compared with the acceptance function obtained from pseudopupil measurements. In spite of the inadequacies of the ray tracing method (exact ray paths, local refractive index gradients and cone surface shape are all approximated) the correspondence is encouragingly good: the estimated half-width ($\Delta\rho$) is 3°, compared with 3.5° for the measured value. Even if the light-guide junction region is not uniform as assumed here, and no light is totally reflected from the cone walls, $\Delta\rho$ will still not be less than 2.5°, which is 6 times the inter-ommatidial angle $\Delta\phi$.

Image Formation in the Lateral Eyes

The procedures used in the last section to work out the internal structure of the medial eye cones were applied to the cones of the lateral eyes. Figure 11 shows interference micrographs of such cones, and Figs. 13 and 14 the central refractive index gradient and focusing properties of a single cone. These cones are different from those of the dorsal eyes in several important respects. The refractive index is high where the cone abuts onto the carapace, and then decreases proximally with a V-shaped profile towards a 'saddle' about a third of the way down the cone (Figs. 12 and 13). Thereafter, however, the refractive index rises again throughout the proximal 2/3rds of the cone, to reach a peak of 1.45 at the proximal end – a value much higher than any encountered in the medial eye cones. Over this region the periphery is less dense than the centre, so that the refractive index contour lines are again V-shaped, but this time the V is inverted (this means that both distal and proximal regions will bend light rays towards the axis). The cone ends bluntly, and the rhabdoms are situated directly behind the proximal tip; there is nothing equivalent to the light-guides of the medial eye cones.

Conceptually, the cones can be thought of as being in three parts. The distal region acts as a converging lens, very much like the cones of the medial eyes, the central section behaves as a weak lens-cylinder, and the proximal section again acts as a converging lens, but with its convex face directed distally. All three regions contribute to focusing to varying de-

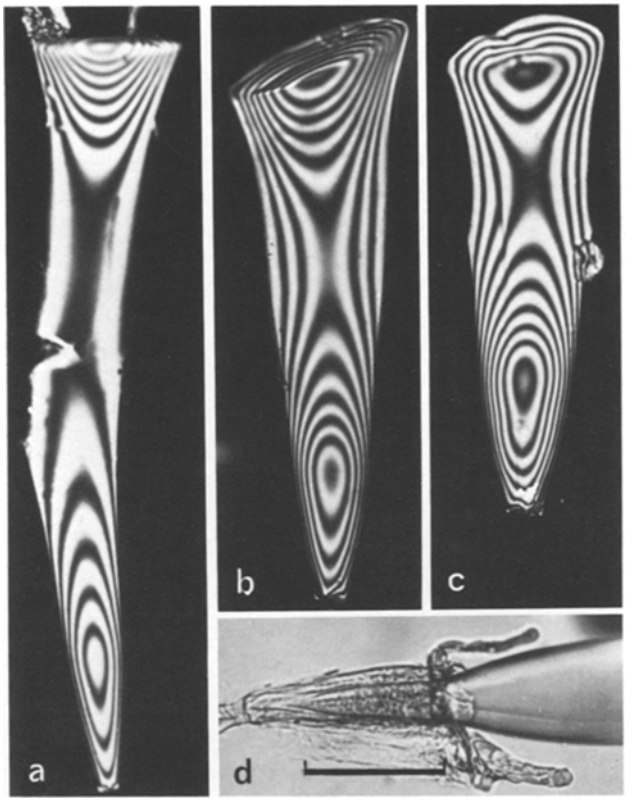

Fig. 11. a–c Three interference micrographs of crystalline cones of different lengths from the lateral eye of *Phronima*. In these nearly cylindrical structures the increased number of fringes distally and proximally indicates higher refractive indices in these regions. Scale on **d**. **d** Normal micrograph of the junction between cone (*right*) and rhabdom showing contact between them. The tapered rhabdom is surrounded by receptor cells and pigment cells distally. *Scale bar*: 100 μm

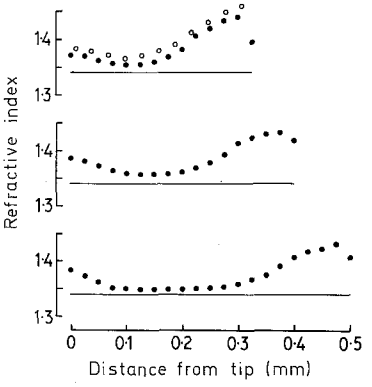

Fig. 12. Average refractive index ($\bar{n}_s$, see Methods) measured along the axis of 3 lateral eye cones of different lengths (*filled circles*). The *open circles* on the *upper figure* give the corrected axial refractive indices from Fig. 13, which are 0.01 to 0.02 higher than the average indices. In all cases there is a high index at both ends of the cones, separated by a low index central section. Distal tip to the left. Lines represent sea water ($n=1.34$)

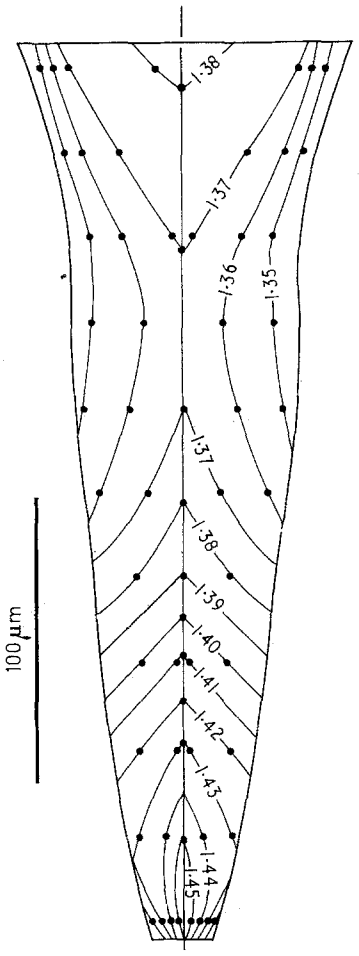

Fig. 13. Refractive index contours in a central section through a cone from the lateral eye of *Phronima*, derived by calculation from a micrograph like that in Fig. 11c. The refractive index is high at both ends, with a 'saddle' in the centre

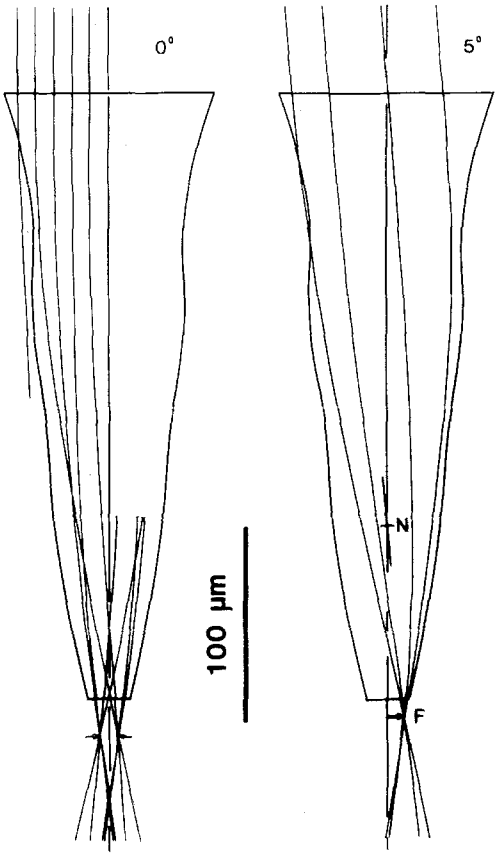

Fig. 14. Paths of axial (*left*) and 5° off-axis rays (*right*) traced through the contours shown in Fig. 13. Parallel rays are focused just below the proximal tip, in the rhabdom (Fig. 11d). The focal length of the whole cone is the distance from nodal point (*N*) to focus (*F*)

grees, and the result of tracing rays through the structure is that the region of best focus lies about 20 µm behind the proximal end of the cone, and just inside the rhabdom (Fig. 14). Because of the converging power of the long proximal section, the focal length of the whole cone is quite short (110 µm in the illustrated case) with the nodal point, determined by tracing off-axis rays, situated about 90 µm in from the proximal tip (Fig. 14). Since the rhabdom diameter in this part of the eye is about 20 µm, the subtense of each rhabdom ($\Delta\rho$) will be 20/110 radians, or 10.4°. As in the medial eye cones, some light will be reflected into the rhabdom from the walls of the cone, and approximate calculations indicate that this will increase $\Delta\rho$ for light entering the rhabdoms to about 15°. This suggests that the acceptance angle of the lateral eye rhabdoms is about $1^1/_2$ times the interommatidial angle (9–12°) which is consistent with the observation that the pseudopupil has a width of 1–2 facets.

The cones in the lateral eyes vary in length by a factor of 2. The basic design appears to be the same, with a high refractive index region at both proximal and distal ends (Fig. 12), and what changes most is the length of the relatively low refractive index region in between. In other amphipods like *Cystisoma* (Fig. 17d) this intermediate region may be drawn out into a narrow rod a mm or more long. It is difficult to assess the effect that lengthening the cone would have on $\Delta\rho$, because the focal length of a combination of two separated lenses – which is effectively what we have here – depends on the focal length of each lens and on their separation (cf. Land 1980b, p. 522). Thus it is quite possible for cones of different overall lengths to have the same focal length and hence similar rhabdom acceptance angles, or alternatively the

focal lengths may vary systematically across the eye. So far there is no evidence either way.

Comparisons of Medial and Lateral Eyes

The cones of both medial and lateral eyes have similar mechanisms for focusing light using inhomogeneous lenses with conical refractive index gradients. However, whereas the medial cones effectively use only one lens which focuses light into a long light-guide, the lateral cones have two such lenses back to back with a low refractive index region in between. Possibly the light-guides of the medial eyes are best regarded as greatly extended homologues of the proximal lenses of the lateral eye cones, but this is not yet clear.

Table 1 compares the optical properties of the two eyes. The absolute sensitivities are calculated from the formula in Land (1980b Eq. 15) which gives the light energy a receptor would be expected to absorb from an extended source of unit luminance ($\Delta\rho$ has been substituted for d/f in the formula to take account of light reflected by the cone walls). In fact the sensitivities differ rather little, in spite of the larger acceptance angles of the lateral eye ommatidia. This is because the apertures are smaller and the rhabdoms shorter in the lateral eyes: Ball's (1977) figures of 350 μm for rhabdom length in the medial eye and 50–200 μm for the lateral eye, taken with the estimate of Bruno et al. (1977) for the absorption coefficient of lobster rhabdoms (0.0067 μm^{-1}), indicate that the medial rhabdoms will absorb 90% of the light entering them, but the lateral rhabdoms only 31–74%. However, the resulting figures for absolute sensitivity (70–313) indicate that both are high sensitivity eyes. They are comparable with moth superposition eyes (*Ephestia*: 82.8), much more sensitive than diurnal insect eyes (bee: 0.318), but considerably less sensitive than the superposition eyes of some deep-water shrimps (*Oplophorus*: 3,303) (all figures from Land 1980b). They are probably more sensitive than any other apposition eyes, with the possible exception of *Limulus* (sensitivity around 300, based on data from Land 1979 and Barlow et al. 1980).

Table 1. Optical properties of the medial and lateral eyes of *Phronima*

		Medial eye	Lateral eye
Aperture of cone	A (μm)	183	100
Focal length of cone	f (μm)	403	110
F-number		2.2	1.1
Diameter of light-guide or rhabdom	d (μm)	17.6	~20
Rhabdom length	x (μm)	350	50–200
Field of view		10.5 × 11°	~180 × 180°
Interommatidial angle	$\Delta\phi$	0.44°	9–12°
Acceptance angle	$\Delta\rho$	3.5°	~15°
Absolute sensitivity $\frac{\pi}{4}\,^2A^2\Delta\rho^2(1-e^{-kx})$	(see note)	70	130–313

Note: The units of sensitivity are area (μm^2). They signify the equivalent area of a totally absorbing surface (outside the eye) receiving light from a source of unit luminance subtending one steradian at the surface. The absorption coefficient (k) is taken as 0.0067 μm^{-1}, the value for the lobster (Bruno et al. 1977). The sensitivity figure is also the multiplying factor for working out the number of photons received by a rhabdom when the number emitted by an extended source is known (see Discussion, Eq. 4)

The real difference between the medial and lateral eyes is not in sensitivity but resolution. This is substantial in terms of acceptance angles ($\Delta\rho$), which differ by a factor of about 4, but the ratio of interommatidial angles ($\Delta\phi$) of around 24 is even more impressive. It means that if a given solid angle of space is sampled by one ommatidium of a lateral eye it would be sampled by 24^2 or 576 ommatidia if a medial eye were viewing it. In fact, since the field of view of the medial eyes is largely binocular the figure would be twice this. A more dramatic way of putting this is that *the entire field of view of the two dorsal eyes, with 800-odd ommatidia, occupies a smaller visual angle than one lateral eye ommatidium.* The problem is that the medial eyes do not resolve as well as they sample. There can be no information about grating-like objects that subtend angles smaller than $\Delta\rho$, which is 8 times larger than the sampling angle $\Delta\phi$. The question of why there might be this extraordinary degree of apparently useless overlap between ommatidial fields of view is the subject of the Discussion.

Discussion

Detecting Small Objects in the Sea

Phronima sedentaria are found at daytime depths of 85–800 m (Thurston 1976) so that the ambient light levels range from weak daylight to complete darkness. Their food apparently consists of other crustaceans and transparent animals – siphonophores or medusae and the tunicates from whose tests they shape the barrels in which they live (Ball 1977). It is a reasonable assumption, therefore, that a major function of vision is to locate objects that are small and/or of low contrast. Downwelling light in the sea is about 200 times brighter than upwelling light, so that it is again a safe assumption that the high resolution medial eyes look upwards, since this will be the best direction

to detect edible objects. Food is sparse at these depths, so it will be advantageous to detect objects as far away as possible. In contrast to the visual world of terrestrial insects, *Phronima*'s world contains no 'background' of structured foliage, which must be resolved if it is to be used in course stabilization, for example. It is thus probably not appropriate to think in the resolving power of the *Phronima* eye in terms of its ability to resolve stripes, as one might for an insect or terrestrial vertebrate, but rather its ability to detect small low-contrast objects. Whilst there is an extensive literature on the optimal design of compound eyes for resolving grating-like objects under different light conditions (rev. Snyder 1979), there has been no corresponding discussion of the way eyes should be organised to detect single small objects on homogeneous backgrounds, which is presumably the task involved here. It is clear that the problems are different because single objects are potentially detectable no matter how small they are relative to the receptor mosaic, provided the receptors are sufficiently sensitive to small brightness changes. With grating-like objects this is not true, and the ability to resolve disappears completely when the pattern becomes finer than the retinal mosaic. Let us now consider what features of an eye are likely to make it suitable for detecting small low contrast objects against a dim background.

Whether or not an object is detectable will depend on the magnitude of the flux decrease in the receptor that receives its image, compared with an adjacent receptor imaging the background. If this decrease is greater than the noise level of the background, due to random photon fluctuations, then the object should be detectable. Making use of the fact that the standard deviation (σ) of photon numbers in a given time sample is equal to $\sqrt{s}$, where s is the average number in the sample, we can write that the condition for detection is:

$$\delta s > \sigma \quad \text{or} \quad \delta s > \sqrt{s}, \tag{1}$$

where δs is the decrement in photon numbers caused by the presence of the object. Dividing by s, and rearranging the expression gives:

$$s > \left(\frac{1}{\delta s/s}\right)^2. \tag{2}$$

$\delta s/s$ is now the relative decrement, or contrast, of the object as seen by a receptor and it will be low if the object is transparent. The expression states, for example, that if the object causes a 10% decrement at one receptor, then the average number of background photons received per receptor must be greater than 100 in a given sampling time.

If the object to be detected is small compared with the acceptance angle of a receptor, i.e. $\Delta\psi < \Delta\rho$ (Fig. 15a), then the contrast seen by the receptor will be reduced in proportion to the ratio of the solid angles subtended by the object and acceptance function, i.e. by $(\Delta\psi/\Delta\rho)^2$. Thus for small objects Eq. (2) becomes:

$$s > \left(\frac{1}{\delta s/s\,(\Delta\psi/\Delta\rho)^2}\right)^2 \quad \text{or} \quad s > \left(\frac{1}{\delta s/s}\right)^2 \cdot \left(\frac{\Delta\rho}{\Delta\psi}\right)^4. \tag{3}$$

It would seem from this expression that the smaller $\Delta\rho$ is, the better. Smaller photon numbers would be needed to detect an object of a given subtense, for example, if $\Delta\rho$ is small.

This, however, is not the complete story, because the number of photons *available* to a receptor (as opposed to those *required* for a particular task) is also a function of $\Delta\rho$, and this must be taken into account if the performance of an eye is to be assessed in terms of its detecting ability. The general formula, based on straight-forward photometric considerations, for calculating the number of photons (s_a) that a receptor will receive from an extended source emitting L photons $\cdot m^{-2} \cdot s^{-1} \cdot sr^{-1}$ is:

$$s_a = L \cdot \left(\frac{\pi}{4}\right)^2 \cdot \left(\frac{A}{f}\right)^2 \cdot d^2 \cdot (1 - e^{-kx}), \tag{4}$$

where A is the aperture diameter of the lens, f is the focal length, d is the receptor diameter, x the receptor length and k the absorption coefficient of the visual pigment. The derivation is given in Land (1980b, p. 483). Since the acceptance angle of a receptor $\Delta\rho$ is approximately equal to d/f, and, if the rhabdoms are long enough, $(1 - e^{-kx})$ approaches 1, Eq. (4) can be rewritten:

$$s_a \simeq L \cdot A^2 \cdot \Delta\rho^2. \tag{5}$$

To work out the smallest object the eye can detect against a background of radiance L we can equate the photons required (Eq. 3) with those available (Eq. 5) giving:

$$\left(\frac{1}{\delta s/s}\right)^2 \cdot \left(\frac{\Delta\rho}{\Delta\psi}\right)^4 = L \cdot A^2 \cdot \Delta\rho^2,$$

or

$$\Delta\psi = \sqrt{\frac{1}{\delta s/s} \cdot \frac{\Delta\rho}{\sqrt{L \cdot A}}}. \tag{6}$$

This states that $\Delta\psi$ will decrease as the square root of the acceptance angle decreases, and as the square root of the facet aperture increases. $\Delta\rho$ should be small and A large for optimal detection. The problem is that in *Phronima*'s medial eye $\Delta\rho$ is *not* small.

The problem can be solved by making one im-

portant ancillary assumption, namely that the signals of individual receptors are shared in such a way that *all receptors whose acceptance angles overlap each other pool their signals* (Fig. 15b). In practice this would mean that about 60 receptors should contribute their signals to each higher order neuron. If this occurs, then each such neuron will receive a maximal signal concerning the presence of an object in one particular direction: if the pooling angle were smaller than the overlap angle the signal would be less than maximal, and if larger the signal would be 'diluted' by background light that does not contain the target. Inspection of Fig. 15b shows that the number of acceptance angles that overlap at any point is $(\Delta\rho/\Delta\phi)^2$, so that Eq. (5) can be rewritten to give the effective photon number (s_p) seen by each pooling neuron. This will be:

$$s_p \simeq L \cdot A^2 \cdot \Delta\rho^4/\Delta\phi^2. \tag{5a}$$

When Eq. (6) is altered appropriately the $\Delta\rho^4$ terms cancel out leaving:

$$\Delta\psi = \sqrt{\frac{1}{\delta s/s} \cdot \frac{\Delta\phi}{\sqrt{L \cdot A}}} \tag{6a}$$

This seems now to be the kind of answer we are seeking, since it says that the ability to detect small objects improves as the *interommatidial* angle $\Delta\phi$ gets smaller, and the ommatidial aperture (A) larger. *Phronima* does appear to have gone to heroic extremes to make $\Delta\phi$ small and A large. The important point is that the size of the acceptance angle ($\Delta\rho$) *no longer matters*.

If this is the explanation for the overlap of acceptance angles in the medial eyes, then an essential prediction is that pooling must occur and an anatomical substrate for pooling should be present. Further, since there is very little overlap between acceptance angles in the lateral eyes, they should not have such a mechanism. There is some anatomical evidence that is at least compatible with these predictions. Between the retina and the lamina of the medial eyes there is an extensive lateral plexus that is probably composed of collaterals of the receptor axons, and this plexus is not present in the projection from the lateral eyes (Fig. 16). It is very tempting to suppose that this is the site of signal pooling, with each receptor contacting the laminar cells corresponding to the 60 surrounding receptors, but the extent of the spread of processes in the plexus is not yet known.

If the argument in this section is essentially correct for *Phronima*, then it should apply to other animals as well. In particular it should be valid for other hyperiids, amongst which there are many other examples of high $\Delta\rho:\Delta\phi$ ratios as judged by the sizes of

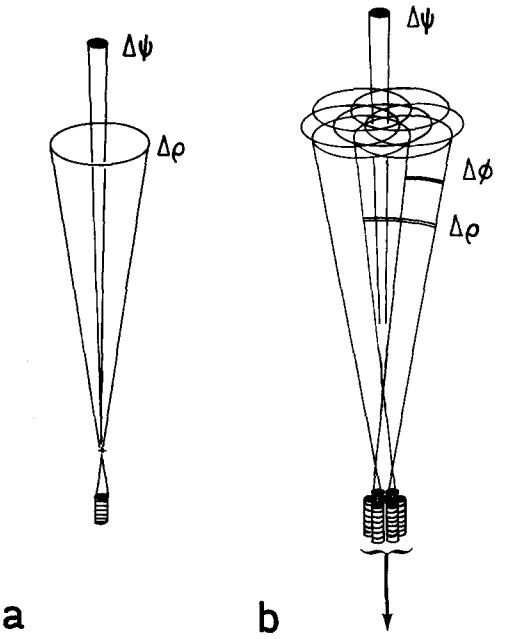

Fig. 15. a Single receptor with acceptance angle $\Delta\rho$ imaging an object subtending a much smaller angle $\Delta\psi$. The contrast seen by the receptor will be lower than that of the object by a factor $(\Delta\psi/\Delta\rho)^2$. See text. **b** Many receptors with overlapping fields viewing the same object. If the acceptance angles are $\Delta\rho$ and the interommatidial angles $\Delta\phi$, the number viewing the same point in space will be $(\Delta\rho/\Delta\phi)^2$. The optimum condition for detecting a small object will be met if all receptors that view the same point pool their signals. See text

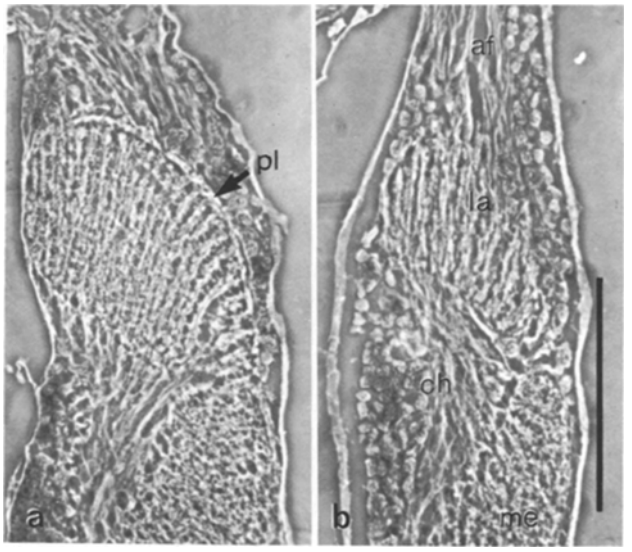

Fig. 16a, b. Region of the lamina (1st synaptic layer) of the medial eye (**a**), and lateral eye (**b**), showing the presence of a lateral plexus over the surface of the lamina in the medial eye only. *af* afferent fibres from retina; *la* lamina; *ch* chiasm; *me* medulla; *pl* plexus. *Scale bar*: 100 μm. Both from the same preparation. 2 μm epoxy sections in phase contrast (fibres lighter than background)

the pseudopupils (all those in Fig. 6 for example). The other feature of some hyperiid eyes that this argument may help to explain is their bizarre shape. *Streetsia* is perhaps the most extreme, with an eye that is so elongated that it is almost cylindrical (photograph in Land 1980b, p. 560). If an arrangement for pooling input signals exists, then this can be tailored to any shape of eye. It will be the geometry of the interconnections between retina and lamina that determines the form of the field of view, rather than the external structure of the eye itself. If the eye is cylindrically extended, and the collecting areas of the laminar neurones are also asymmetrically extended along the cylinder's axis, then these neurones can still be arranged so that each one views a unique direction in space just as in Fig. 15b. With such a mechanism the usual constraints that tend to make compound eyes more or less spherical can be, and apparently have been, relaxed because it is no longer necessary for acceptance angles to be contiguous and non-overlapping.

A final situation in which a pooling mechanism of this kind might be useful is in eyes where the image is poor for optical reasons. This might apply to the superposition eyes of macruran decapods, euphausiids and mysids where, because of the wide angle of the cone of light reaching the retina, it is inevitable that many receptors will be stimulated by light from a single point in object space. This is exactly equivalent to having a high $\Delta\rho:\Delta\phi$ ratio, and the same considerations would apply as in *Phronima*. An arrangement for pooling the signals from all receptors that occupy the blur circle produced by a point source would improve detection without further worsening resolution. It must be stressed again that signal pooling as proposed here is of no value in the resolution of textured backgrounds, where there is no substitute for high resolution (small $\Delta\rho$) optics.

The only terrestrial situation that is at all like that in the sea, where small objects must be seen against unstructured backgrounds, occurs in swarming insects where males detect females against the sky, often at quite low light levels. Amongst the swarming diptera there is no suggestion that any pooling is employed beyond that involved in the 'neural superposition' mechanism itself (Kirschfeld 1979). In the mayflies, however, where the males have enlarged eyes that probably use a superposition mechanism (Horridge 1976; Horridge and McLean 1978), a pooling mechanism like that proposed for *Phronima* might well be employed.

Long Focal Length Lens Cylinders

The medial eye lenses of *Phronima* seem to have evolved to provide a long focal length. The refractive index range involved is small compared with a *Limulus* lens cylinder (Land 1979), and the use of a V-shaped gradient, rather than one in which refractive index contours are parallel to the axis as in moths (Kunze 1979), both mean that the rays are bent less than they might be in a device of the same length. These are thus lens cylinders of low power and, concomitantly, high *F*-number. The reason for this in *Phronima* seems clear: a high power lens cylinder would give rise to rays converging at too great an angle to enter the light-guide by total internal reflection, and the same would hold true if the light guide were a rhabdom with a refractive index in the range 1.37–1.40. Powerful lens cylinders of the kind envisioned by Exner may not be generally appropriate for apposition eyes, and it may turn out that in other apposition eyes without effective corneas – crabs for example, and some mantids with flat corneas (Horridge and Duelli 1979) – 'weakened' lens cylinders like those of *Phronima* may turn out to be the rule. *Limulus* is the exception, presumably because its receptor complex is ball-shaped, and does not have to behave as a rhabdom light guide.

Double Eyes and Camouflage

Most hyperiids are exceedingly transparent, and often the only part of the animal which is at all easy to see is the retina itself. Making the retina as small as possible, by condensing it down into a small spot, might therefore be a way of improving the camouflage of the animal as a whole. This applies particularly to the medial eyes where the optical surface is large, not only in *Phronima*, but in two of the other species (*Platyscelus* and *Phrosina*) shown in Fig. 6. In all 3 cases the retina of the medial eye is a small spot at some distance from the optical array, and separated also from the equally small retina of the lateral eyes. The interesting exception is *Cystisoma* (Fig. 17a) which lacks lateral eyes, and where the retina of the medial eyes is not a compact structure as in *Phronima*, but a curtain-like layer co-extensive with the optical array, and only just below it. As in the medial eye of *Phronima*, the field of view is very small and almost entirely binocular. There is very little screening pigment, so that the pseudopupil is a light orange colour, and best seen 'antidromically' (Franceschini and Kirschfeld 1971) by illuminating the retina from below (Fig. 17b). An excellent colour photograph of this rare animal can be found in George and George (1979; plate 65).

The fact that the *Cystisoma* eye is similar in optical properties to the medial eye of *Phronima*, but lacks the long light-guides, confirms the view that those light-guides are not *optically* important: the retina could equally well be situated just below the crystal-

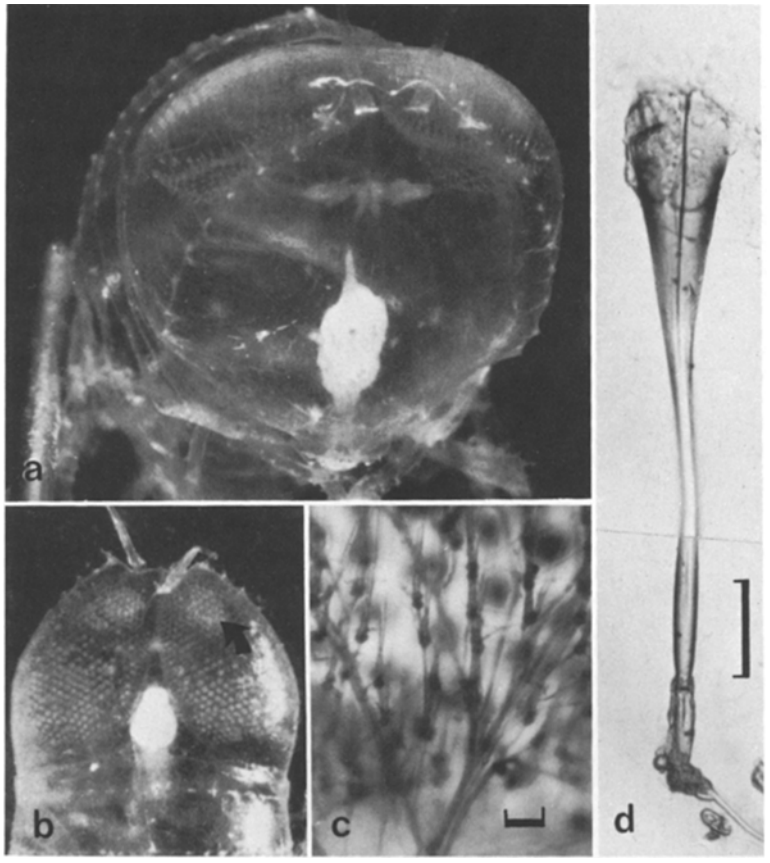

Fig. 17. a Head of *Cystisoma*. There are no lateral eyes, and the retina of the medial eyes is the curtain-like structure just below the dorsal surface. Living animal. Head diameter 7 mm.
b Head of the same animal from above, showing facets and the two antidromically illuminated pseudopupils (*arrow*) which glow from light emitted back from the rhabdoms.
c View of the retina from below, showing the loosely spaced rhabdoms and fibres of the optic nerve innervating them. *Scale bar*: 100 μm.
d Single cone from *Cystisoma*, ending in the rhabdom with a nerve leaving it. The whole structure is less than 1 mm long (cf. Fig. 2b) and the cones have a refractive index structure like 'long' cones from the lateral eyes of *Phronima*, with distal and proximal lenses rather than a proximal light-guide. *Scale bar*: 100 μm

line cones. Their function must be to provide the link between the large optical surface and small compact retina, thus improving camouflage, as Ball (1977) has already suggested. Why, then, does *Cystisoma not* use this mechanism? The answer is probably that *Cystisoma* uses an alternative strategy, making the retina as transparent as possible by leaving out all screening pigment (Fig. 17c, d). As far as overall visibility is concerned, the two strategies may be equally effective. For example, if the retinal diameter is decreased by a factor of 10 this is equivalent to reducing the overall optical density of the retina by a factor of 100 – a situation that could be achieved by having 10 μm wide naked rhabdoms 100 μm apart – roughly as in *Cystisoma* (Fig. 17c). This solution, however, is only possible where the amount of unfocused light reaching the retina is negligible, and so may be confined to very deep-living creatures like *Cystisoma*. At moderate light levels making the retina compact is a better solution. Another reason for the light-guide arrangement in *Phronima* may be simply that it is convenient for the retinae of medial and lateral eyes to lie close to each other so that they can share the same optic neuropiles. In *Cystisoma* this wouldn't matter, as there are no lateral eyes.

The remaining problem with hyperiid eyes, as with other double-eyed Crustacea like certain euphausiids (Land et al. 1979), is the function of the lateral eyes. They are slightly more sensitive than the medial eyes in terms of their photon capture rate, but this is not enough to make up for the 200-fold difference in the intensities of upwelling and downwelling light. Their resolution is much worse, and their ability to detect small objects (Eq. 6a) will be worse by a factor of 8 (i.e. other things being equal an object would need to be 8 times wider to be detected by the lateral eye). Unlike the medial eye the lateral eyes do not seem to be specially adapted for any particular task. They simply provide low quality all-round vision for an animal that has only space in its head for a limited region of acute vision. The probable reason why *Cystisoma* has dispensed with lateral eyes is that at depths greater than about 700 m there is not enough light to see in any direction other than upwards. Again there is a parallel here in euphausiids with superposition eyes: *Nematobrachion boopis* has almost lost the ventral part of its double eye (Land et al. 1979). Many deep-sea fish have similarly dispensed with the lower part of their field of view.

My thanks are due to Peter Herring of the Institute of Oceanographic Sciences, Wormley, U.K. who organized the Discovery cruises, and the Michael Thurston, also of the I.O.S. for taxonomic and general advice on amphipods. Jonathan Ashmore, Ian Russell and Jochen Zeil all made helpful criticisms of the manuscript,

which was typed by Sally Byatt. The research was funded by the N.E.R.C. (at sea) and the S.R.C. (at Sussex).

References

Ball EE (1977) Fine structure of the compound eyes of the midwater amphipod *Phronima* in relation to behavior and habitat. Tissue Cell 9:521–536

Barlow RB, Chamberlain SC, Levinson JZ (1980) *Limulus* brain modulates the structure and function of the lateral eyes. Science 210:1037–1039

Bowman TE, Gruner HE (1973) The families and genera of Hyperiidea (Crustacea: Amphipoda). Smithson Contrib Zool, vol 146. Smithsonian Institute Press, Washington, DC

Bruno MS, Barnes SN, Goldsmith TS (1977) The visual pigment and visual cycle of the lobster *Homarus*. J Comp Physiol 120:123–142

Claus C (1879) Der Organismus der Phronimiden. Arb Zool Inst Univ Wien 2:1–88

Exner S (1891) Die Physiologie der facettierten Augen von Krebsen und Insecten. Deuticke, Leipzig Wien

Franceschini N, Kirschfeld K (1971) Les phénomènes de pseudopupille dans l'oeil composé de *Drosophila*. Kybernetik 9:159–182

George D, George J (1979) Marine life. Wiley, New York

Hausen K (1973) Die Brechungsindices im Kristallkegel der Mehlmotte *Ephestia kühniella*. J Comp Physiol 82:365–378

Horridge GA (1976) The ommatidium of the dorsal eye of *Cloeon* as a specialization for photoreisomerization. Proc R Soc Lond [Biol] 193:17–29

Horridge GA (1978) The separation of visual axes in apposition compound eyes. Philos Trans R Soc Lond [Biol] 285:1–59

Horridge GA, Duelli P (1979) Anatomy of the regional differences in the eye of the mantis *Cuilfina*. J Exp Biol 80:165–190

Horridge GA, McLean M (1978) The dorsal eye of the mayfly *Atalophlebia*. Proc R Soc Lond [Biol] 200:137–150

Kirschfeld K (1979) The visual system of the fly: physiological optics and functional anatomy as related to behavior. In: Schmitt FO, Worden FG (eds) The neurosciences 4th study program. M.I.T. Press, Cambridge, MA, pp 297–310

Koizumi K, Ikeda Y, Kitano I, Furukawa M, Sumimoto T (1974) New light-focusing fibres made by a continuous process. Appl Opt 13:255–260

Kunze P (1979) Apposition and superposition eyes. In: Autrum H (ed) Handbook of sensory physiology, vol VII/6A. Springer, Berlin Heidelberg New York, pp 441–502

Land MF (1979) The optical mechanism of the eye of *Limulus*. Nature 280:396–397

Land MF (1980a) Compound eyes: old and new optical mechanisms. Nature 287:681–686

Land MF (1980b) Optics and vision in invertebrates. In: Autrum H (ed) Handbook of sensory physiology, vol VII/B. Springer, Berlin Heidelberg New York, pp 471–592

Land MF, Burton FA, Meyer-Rochow VB (1979) The optical geometry of euphausiid eyes. J Comp Physiol 130:49–62

Lockett NA (1977) Adaptations to the deep-sea environment. In: Crescitelli F (ed) Handbook of sensory physiology, vol VII/5. Springer, Berlin Heidelberg New York, pp 67–192

Lythgoe JN (1979) Ecology of vision. Clarendon Press, Oxford

Marshall NB (1954) Aspects of deep-sea biology. Hutchinson, London

Meggitt S, Meyer-Rochow VB (1975) Two calculations on optically non-homogeneous lenses. In: Horridge GA (ed) The compound eye and vision of insects. Clarendon Press, Oxford, pp 314–320

Rossel S (1979) Regional differences in photoreceptor performance in the eye of the praying mantis. J Comp Physiol 131:95–112

Sherk TE (1978) Development of the compound eyes of dragonflies (Odonata) III. Adult compound eyes. J Exp Zool 203:61–79

Snyder AW (1979) The physics of compound eyes. In: Autrum H (ed) Handbook of sensory physiology, vol VII/6A. Springer, Berlin Heidelberg New York, pp 225–313

Stavenga DG (1979) Pseudopupils of compound eyes. In: Autrum H (ed) Handbook of sensory physiology, vol VII/6A. Springer, Berlin Heidelberg New York, pp 357–439

Thurston MH (1976) The vertical distribution and diurnal migration of the Crustacea Amphipoda collected during the SOND cruise, 1965. J Mar Biol Ass UK 56:383–470